

Solar coronal heating by forced magnetic reconnection: Multiple reconnection events

Rekha Jain^{a)}

Department of Applied Mathematics, University of Sheffield, Sheffield S3 7RH, United Kingdom

Philippa Browning^{b)}

Department of Physics, UMIST, Manchester M60 1QD, United Kingdom

K. Kusano^{c)}

Graduate School of Advanced Sciences of Matter, Hiroshima University, Japan

(Received 23 July 2004; accepted 20 October 2004; published online 16 December 2004)

Magnetic reconnection is a strong candidate for a coronal heating mechanism, and heating by forced magnetic reconnection is investigated here. Two dimensional, nonlinear magnetohydrodynamic simulations are used to investigate forced magnetic reconnection in a compressible plasma. The reconnection occurs when a sheared force-free field is perturbed by a slow disturbance (pulse) at the boundary which is representative of the solar corona where the reconnection is induced by the photospheric motions. The case of driving by successive pulses, which generate a series of heating events which may interact with each other, is considered. This is in order to model the heating of the corona by a series of *nanoflare* events. For small perturbations, the simulation results are consistent with the previous analytic theory based on linear approach where a current sheet is formed initially at the resonant surface followed by reconnection and then release of magnetic energy. For large amplitude perturbations, or close to the threshold for tearing instability, the system exhibits strong nonlinear aspects. Following the second driving pulse, the current sheet expands along the separatrix before relaxing to a reconnective equilibrium and releasing even more magnetic energy for the same amplitude perturbation. © 2005 American Institute of Physics. [DOI: 10.1063/1.1831278]

I. INTRODUCTION

It has been known for several decades that the Sun's corona is heated to millions of degrees. However, which physical process can keep supplying this kind of heating is an interesting question which is yet to be answered,^{1–4} although evidently the coronal heating mechanism is crucially dependent on the strong coronal magnetic field. In recent years, much international effort has been focused on acquiring high resolution data using Yohkoh, Solar and Heliospheric Observatory (SOHO), Transition Region and Coronal Explorer (TRACE) and making parallel advances in theoretical modeling to explain the heating mechanism and predict its observable signatures.

It is now accepted that the Sun's corona is highly dynamic and the heating process could be sporadic. It has been suggested that small scale events known as *nanoflares*,⁵ occurring frequently in large numbers could account for the energy needed to maintain the hot solar corona. Thus, the underlying physical processes should be similar to those in larger energy release events, namely, flares. In highly conducting plasmas, magnetic reconnection is closely associated with the release of magnetic energy and plasma heating, in particular, in solar flares, as well as in many other contexts both in astrophysical and laboratory plasmas.⁶ Reconnection allows the magnetic topology to change, and magnetic en-

ergy to be converted into thermal and kinetic energy, on time scales which are far more rapid than the global ohmic diffusion time. One form of magnetic reconnection, which can occur as a result of the resistive magnetohydrodynamic (MHD) instability, is the tearing mode. Another, of more relevance to coronal heating, and of interest here, is forced reconnection, when the necessary prerequisite for the process, a current sheet, is generated by external deformation of the initially smooth magnetic field. Forced magnetic reconnection in the solar corona is very likely to be initiated by the displacement of the photospheric footpoints, though it may also be triggered by newly emerging flux or by coronal disturbances.

The forced reconnection scenario was pioneered by an analysis of the "Taylor problem,"⁷ in which a slab plasma with a field reversal is subjected to a sinusoidal boundary disturbance, driving current sheet formation, and subsequent reconnection at the neutral sheet. This model has since been the subject of considerable study both as a fundamental problem in plasma physics and with application mainly in the formation of magnetic islands and their effects on confinement in magnetically confined fusion devices.^{8–11} Numerical simulations of the nonlinear phase have been carried out in Ref. 12.

In the context of the solar corona, a more relevant configuration is a sheared force-free field rather than a neutral sheet, and the interest is more in the energetics of the process. Reference 13 studied forced magnetic reconnection using a linear approach (analytical model) where they consid-

^{a)}Electronic mail: R.Jain@sheffield.ac.uk

^{b)}Electronic mail: P.Browning@umist.ac.uk

^{c)}Electronic mail: kusano@hiroshima-u.ac.jp

ered a low- β plasma embedded in a sheared force-free field. It was found that when the equilibrium was perturbed by a boundary displacement of the form $\delta_o \cos ky$, the field initially evolves (on an Alfvénic time scale) to an “ideal equilibrium” which has a current sheet at the resonant surface. The perturbed flux in this state is denoted by $\psi_1^{(i)}$. Thus, the total flux function in the ideal equilibrium is the sum of the unperturbed and perturbed flux functions, i.e., $\psi = \psi_o + \psi_1^{(i)}$. After a longer time when resistivity becomes important, reconnection occurs and the system relaxes to a lower energy “reconnected equilibrium” containing magnetic islands. The total flux in reconnective equilibrium state is given by $\psi = \psi_o + \psi_1^{(r)}$. The transition time for the system to evolve from the ideal equilibrium to the reconnected equilibrium is estimated to be $\tau_\eta S^{-1/2}$, where τ_η ($\propto 1/\eta$) is the global resistive time scale and $S = (\tau_\eta/\tau_A)$; τ_A is the Alfvén transit time] is the Lundquist number.¹³ The energy released as heat is the magnetic energy difference between the equilibrium with the current sheet and the equilibrium with magnetic islands, which is found to be $\Delta E_M \propto \delta_o^2 f(\alpha, k)$, where α is the shear in the initial equilibrium. This energy release can be larger than the energy input from the driving disturbance, as some of the stored energy of the initial field is dissipated. The driving perturbation is thus a trigger, rather than the primary source of heating. The heating can become large even for small boundary displacements, and formally diverges at the instability threshold for tearing instability $(\alpha^2 - k^2)^{1/2} < \pi$. Reference 14 also studied continuous plasma heating by considering an interplay between the periodic external driving and internal reconnection. The effective reconnection time scale and the plasma heating rate were derived suggesting that the most effective heating is obtained when the time scale of the external driver is comparable to that of the effective reconnection.

Further investigations were carried out in Ref. 15 to study the nonlinear dynamics of forced reconnection in a sheared field. The simulations using a two-dimensional (2D) magnetohydrodynamics (MHD) mode were carried out applying a slow transient displacement,

$$v(z=0, t) = \begin{cases} -(\delta_o/\tau) \cos ky \hat{z} & \text{if } 0 \leq t \leq 10 \\ 0 & \text{otherwise,} \end{cases} \quad (1)$$

at one boundary ($z=0$), where $\tau=10\tau_A$ is the pulse duration. These numerical results show close agreement with the linear theory¹³ only for large or intermediate k (e.g., $k=2\pi/3$) and small δ_o . For smaller k , and larger δ_o (≥ 0.05), the nonlinear effects, which reduce the energy release from that predicted by linear theory, were found to be quite important in the simulations. These nonlinear effects are more pronounced when the shear in the field is close to the tearing instability threshold. Beyond this, linear theory breaks down as mentioned above and simulations show even stronger nonlinear effects, in particular, predicting a large but finite energy release. According to the linear theory, the magnetic island width scales as $\Delta W \propto \delta_o^{1/2}$, so even for small perturbations, ΔW can be quite large. The simulation results of Ref. 15 found close agreement from the linear theory for small δ_o (< 0.05), but for large δ_o the island widths are found to be

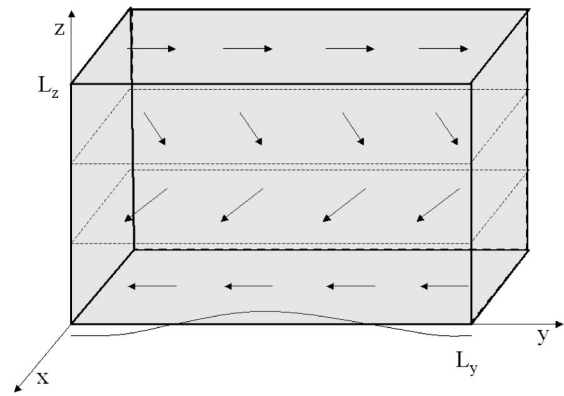


FIG. 1. The simulation domain where L_y and L_z represent the length along the y and z axis. The arrows indicate the rotation of the magnetic field with the z coordinate. The perturbation is applied on $z=0$ plane.

narrower in the simulations due to nonlinear saturation of the reconnection, which is influenced by the interaction between the finite sized island and the boundary.

Heating in the solar corona is believed to be due to superposition of many individual heating events, which may or may not be independent of one another. This is the essence of the nanoflare scenario.⁵ Thus, it is interesting to investigate the nonlinear dynamics of forced magnetic reconnection considering the interaction of multiple events. Here we further develop the simulations of Ref. 15 to study the effect of more than one driving pulse at the boundary, focusing on the energetics. We consider, as in previous work, that the field is initially subjected to a transient boundary disturbance which triggers current sheet formation and a reconnection event, releasing (usually) some of the stored energy of the initial field. At a later time, perhaps before the relaxation is complete, a further pulse triggers a second reconnection and further energy release. It should be noted that the final state of the field (for a single forced reconnection event) is naturally different from the initial state. Hence, a second pulse, even if widely separated from the first in time, could have quite a different heating effect from the first. In principle, the process might repeat with a series of driving pulses and consequent heating events, but we focus here mainly on the simplest case of two successive pulses. In Sec. II we describe the numerical model, presenting the results and comparing with the linear theory, which can make some predictions about the effect of successive pulses in Sec. III. The conclusions are outlined in Sec. IV.

II. NUMERICAL MODEL

A. Description of model

The simulation domain consists of a rectangular region $0 < y < L_y$ and $0 < z < L_z$ and is shown in Fig. 1.

The initial magnetic field is given by a linear one-dimensional sheared force-free field:

$$\begin{pmatrix} B_x \\ B_y \\ B_z \end{pmatrix}(z, t=0) = B_o \begin{pmatrix} \cos \left[\alpha \left(z - \frac{L_z}{2} \right) \right] \\ \sin \left[\alpha \left(z - \frac{L_z}{2} \right) \right] \\ 0 \end{pmatrix}, \quad (2)$$

where B_o and α are constants with α as the shear in the field. When this field is perturbed with wave vector in the y direction at the boundary surface $z=0$, the midplane of the simulation domain corresponding to $z=0.5L_z$ is a resonant surface where the magnetic field in the y direction vanishes ($\mathbf{k} \cdot \mathbf{B}_o = 0$) and a current sheet may be formed at this midplane for all values of α .

We consider compressible plasma governed by the following set of equations described in a nondimensional form:

$$\frac{\partial \mathbf{v}}{\partial t} + \mathbf{v} \cdot \nabla \mathbf{v} = \rho^{-1} [-\nabla p + \mathbf{J} \times \mathbf{B} + \nu \nabla^2 \mathbf{v}], \quad (3)$$

$$\frac{\partial \rho}{\partial t} + \rho \nabla \cdot \mathbf{v} + \mathbf{v} \cdot \nabla \rho = 0, \quad (4)$$

$$\frac{\partial p}{\partial t} = -(\gamma - 1)p \nabla \cdot \mathbf{v} - \nabla \cdot (\rho \mathbf{v}), \quad (5)$$

$$\frac{\partial \mathbf{A}}{\partial t} = (\mathbf{v} \times \mathbf{B}) - \eta(\mathbf{J} - \mathbf{J}_o), \quad (6)$$

$$\mathbf{B} = \nabla \times \mathbf{A}, \quad (7)$$

$$\mathbf{J} = \nabla \times \mathbf{B}, \quad (8)$$

where the pressure p evolves adiabatically. Here, the density ρ , velocity \mathbf{v} , vector potential \mathbf{A} , magnetic field \mathbf{B} , electric current \mathbf{J} , time t , viscosity ν , and resistivity η are normalized by ρ_o , Alfvén velocity $v_A = (B_o) / \sqrt{\mu_o \rho_o}$, $L_z B_o$, B_o , $(B_o / \mu_o L_z)$, Alfvén time $\tau_A = (L_z / v_A)$, (L_z^2 / τ_A) , $(\mu_o / L_z^2 \tau_A)$, respectively. As in Ref. 15, an external field $\eta \mathbf{J}_o$ is added to Eq. (6), where $\mathbf{J}_o = [\nabla \times \mathbf{B}(z, t=0)]$ is the current density in the initial state. It is used for compensating the global resistive diffusion (due to the relatively low magnetic Reynolds number, $S \sim 10^4$ considered in the simulations) in the initial equilibrium. In the case of solar corona, the dynamics is usually dominated by the magnetic pressure. Thus, the parameter β_o , defined as the ratio of gas to magnetic pressure, is generally considered small. In the following results, $\beta_o = 0.1$ unless otherwise stated.

The velocity at the boundary ($z=0$) is perturbed with the following pulses applied at t_{pulse} :

$$v(z=0, t) = \begin{cases} -\delta_o \left(\frac{\omega}{2\pi} \right) (1 - \cos \omega t) \cos ky \hat{z} & \text{if } t_{pulse} \leq t \leq \frac{2\pi}{\omega} + t_{pulse} \\ 0 & \text{if } t > \frac{2\pi}{\omega} + t_{pulse}, \end{cases} \quad (9)$$

where $k = (2\pi) / L_y$. Here, ω and δ_o are the width and amplitude of the pulse, respectively (at the end of the pulse, the boundary is displaced by $\delta_o \cos ky$). The time dependence is chosen to give a smooth variation but, in fact, as expected from linear theory, the subsequent dynamics depend almost entirely on the total displacement ($\delta = \int v dt$) and the pulse time dependence has little effect. With this choice of pulse displacement, we aim to simulate a perturbation similar to those expected in the solar corona. It could, for example, represent a displacement by an exploding granule at the footpoint of the photospheric line-tied coronal magnetic loop. The velocity at the opposite boundary is assumed to be $v(z = L_z, t) = 0$ and there are periodic conditions at $y=0$ and L_y . The numerical code used to solve Eqs. (3)–(8) is based on a two point centered finite difference approximation and the Runge-Kutta-Gill time integration method.¹⁶ The grid numbers are 128×256 along y and z directions and the points are uniformly spaced across the domain.

B. Single driving pulse revisited

Although the primary interest here is on the effects of repeated driving pulses, we first revisit the case of a single

driving pulse^{13,15} in order to gain further understanding of the code and its results, and for comparison with the multiple pulse case. We consider the case when $2\pi/\omega = 10$, i.e., the perturbation comes to rest after ten Alfvén times (the duration is not important so long as it is large compared with τ_A and small compared with reconnection time scale τ_R). The other parameters in their nondimensional units are fixed: $\alpha = 3\pi/4$, $k = 2\pi/3$, $\eta = 10^{-4}$, $\nu = 10^{-4}$, $L_y = 3$, $L_z = 1$.

In Fig. 2, we show three different time snapshots of the x component of the current density J_x (in gray scale) and the flux function A_x (in contours) for $\delta_o = 0.1$ and $\beta_o = 0.1$. We can see that initially a current sheet is formed at the resonant surface $z=0.5$ and the flux contours follow the perturbation of the boundary. As the time progresses, the current sheet is relaxed and the magnetic islands are formed.

Let us now consider the detailed energy balance. All the other parameters are fixed as above. The averaged Poynting flux across the boundary $z=0$ is

$$F_p = \frac{1}{L_y} \int_0^{L_y} (B_x^2 + B_y^2) v_z(z=0) dy. \quad (10)$$

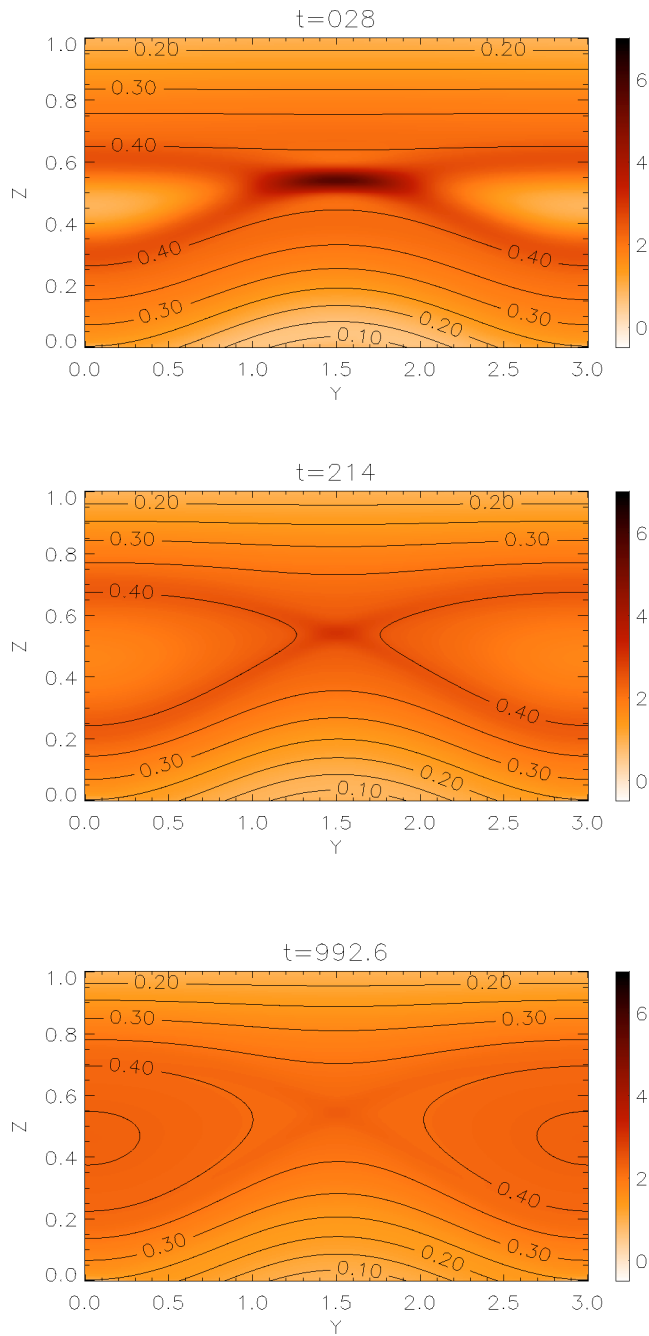


FIG. 2. (Color online). The current density J_x (gray scale) and the flux function A_x (contours) in the simulation domain for $\delta_o=0.1$, $\beta_o=0.1$. Each panel represents different times t as shown.

The average (over the simulation domain) magnetic (E_M) and kinetic (E_K) energies are computed as follows:

$$E_M = \frac{1}{L_y L_z} \int_0^{L_y} \int_0^{L_z} \frac{B^2}{2}(y, z, t) dz dy, \quad (11)$$

$$E_K = \frac{1}{L_y L_z} \int_0^{L_y} \int_0^{L_z} \frac{\rho v^2}{2}(y, z, t) dz dy. \quad (12)$$

Thus, $E_M(t=0)=B_o^2/2=0.5$ and $E_K(t=0)=0$.

The Ohmic dissipation rate is

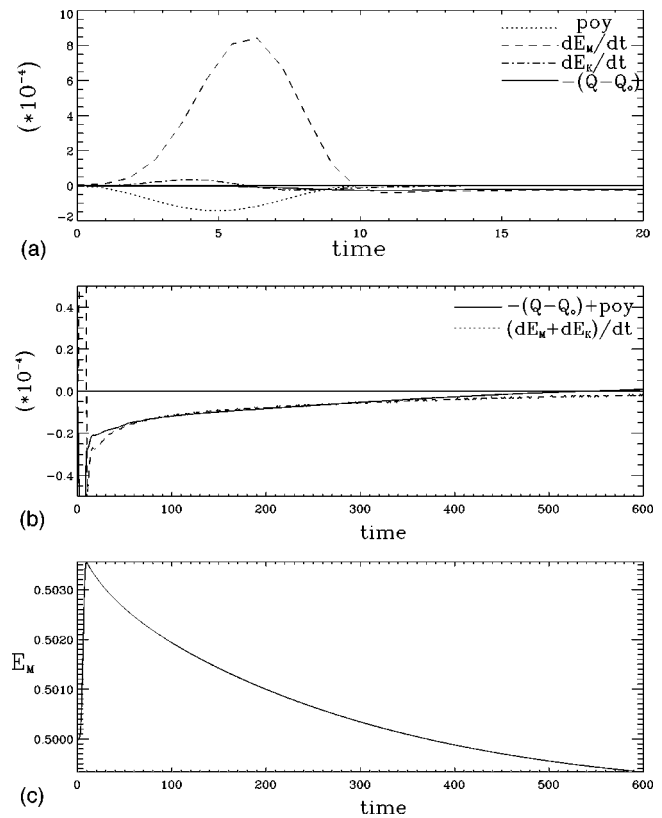


FIG. 3. Various quantities as a function of time: (a) Poynting flux (poy), denoted by small dashed line; derivative of magnetic (E_M) energy, denoted by long dashed line; derivative of kinetic (E_K) energy, denoted by dot-dashed line; dissipation rate $(Q-Q_o)$; where Q_o at $t=0$, denoted by solid line. (b) $-(Q-Q_o)+poy$ denoted by solid line and the derivative of the total energy $[(dE_M/dt)+(dE_K/dt)]$ denoted by dashed line. (c) Averaged magnetic energy, E_M denoted by solid line.

$$Q = \frac{\eta}{L_y L_z} \int_0^{L_y} \int_0^{L_z} [J_x^2(y, z, t) + J_y^2(y, z, t) + J_z^2(y, z, t)] dz dy, \quad (13)$$

such that at $t=0$,

$$Q(t=0) = Q_o = \frac{\eta}{L_y L_z} \int_0^{L_y} \int_0^{L_z} [J_{ox}^2 + J_{oy}^2 + J_{oz}^2] dz dy,$$

with $J_{ox}^2 + J_{oy}^2 + J_{oz}^2 = (\alpha B_o)^2$. Thus, for our choice of parameters, $Q_o = 5.55161 \times 10^{-4}$.

In Fig. 3, we plot these quantities as a function of time. It can be clearly seen [Fig. 3(a)] that the kinetic energy is insignificant compared to the magnetic energy. As expected, the sum of Poynting flux and the dissipation rate is equal to the sum of derivatives of kinetic and magnetic energies [Fig. 3(b)]. The magnetic energy [see Fig. 3(c)] increases initially during the external perturbation ($0 < t \leq 10$) but then it relaxes and approaches a final value which is lower than the initial state ($t=0$, $E_M=0.5$). The maximum energy immediately after $t=10$ corresponds to the energy of an ideal MHD equilibrium while the energy in the final state is the resistive MHD equilibrium, where magnetic reconnection has progressed sufficiently.¹⁵ Thus, the energy dissipated, which is the energy available for heating the plasma, is the difference

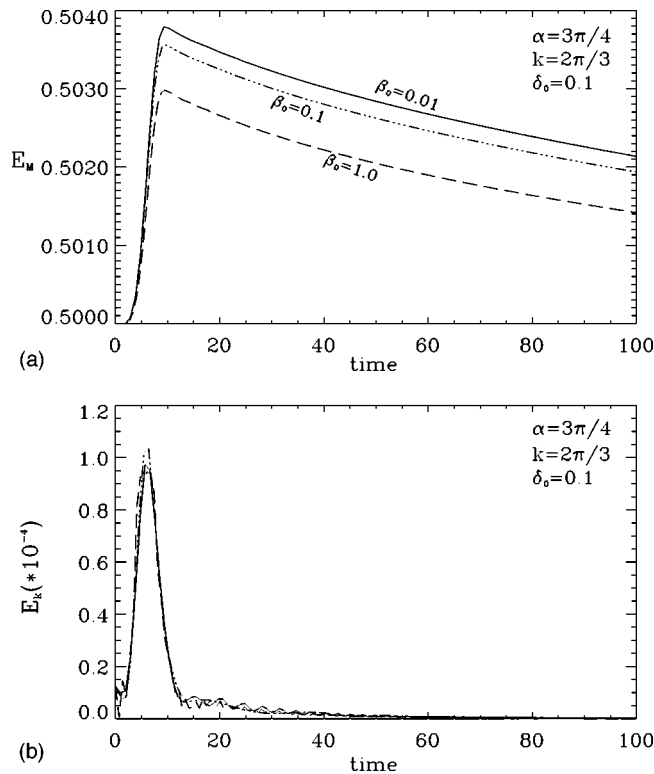


FIG. 4. Averaged (a) magnetic energy E_M (b) kinetic energy E_K as a function of time for three values of $\beta_o=0.01$ (solid), 0.1 (dot-dashed), 1.0 (dashed) for a given α , k , and δ_o .

between the energy of the two equilibria. Thus, some energy of the initial equilibrium is extracted after the perturbation, which is consistent with the prediction of linear theory¹³ and previous simulations.¹⁵ In this paper, we will study the effect of various parameters on the energy release.

Figure 4 shows the averaged (over the simulation domain), magnetic (top panel), and kinetic (bottom panel) energies as a function of time for three different values of β_o . Note that there is a period of dynamic activity as the boundary moves and the current sheet forms (although E_K is still small compared with E_M) which dies away quite rapidly. As β_o increases, the magnetic energy E_M decreases but the kinetic energy E_K remains unchanged. The reduction in E_M with increasing β_o is due to the fact that a part of the energy flux supplied by the boundary perturbation is absorbed by the compressible plasma as the thermal energy. We shall assume $\beta_o=0.1$ and since the kinetic energy is insignificant compared to magnetic energy, we will only consider magnetic energy changes in what follows.

Finally, we consider the effect of varying δ_o which signifies the change in the magnitude of the perturbation, keeping other parameters the same. The magnetic energy E_M for three values of δ_o (0.05, 0.1, 0.2) is plotted as a function of time in Fig. 5(a). As expected, the larger the magnitude of the perturbation (and hence larger Poynting flux), the larger is the magnetic energy increase due to the disturbance. Following the linear theory,¹³ where it was shown that the magnetic energy release is proportional to δ_o^2 , we plot in Fig. 5(b), the quantity $\Delta E_M [E_M - E_M(t=0)] / \delta_o^2$ as a function of time. This enables us to see the effect of nonlinearity as time

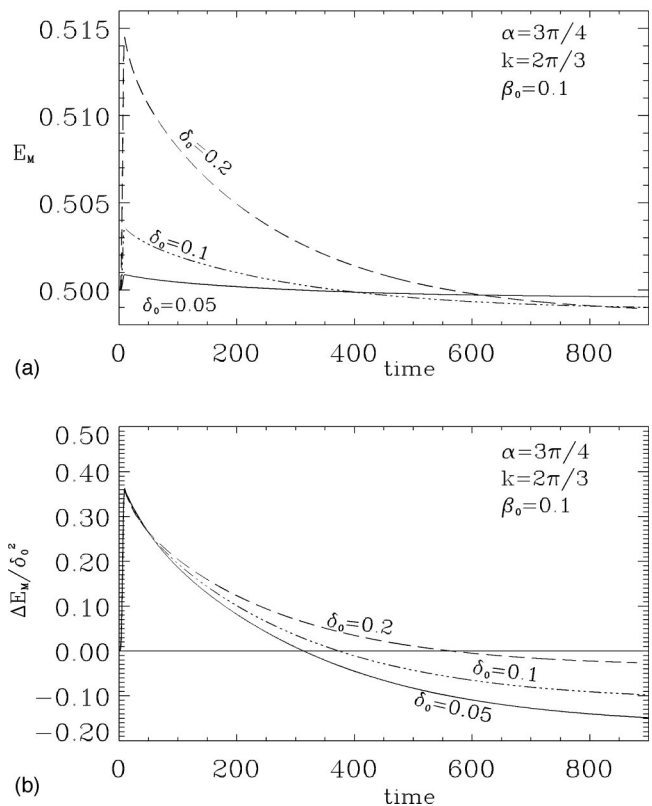


FIG. 5. (a) Averaged magnetic energy E_M as a function of time for three values of $\delta_o=0.05$ (solid), 0.1 (dot-dashed), 0.2 (dashed) for a given α , k , and β_o . (b) $\Delta E_M [E_M - E_M(t=0)] / \delta_o^2$ as a function of time.

progresses. It can be clearly seen from Fig. 5(b) that the initial stages can be described by linear theory but just after $t=50$, nonlinearity in $\mathbf{v} \times \mathbf{B}$ term in Eq. (6) becomes important and as time progresses, the nonlinearity becomes more pronounced for larger δ_o . Thus the energy release (the difference between the energy after the pulse and that of the reconnective field) is affected by nonlinearities.

III. MULTIPLE PULSES

A single reconnective scenario has proved very useful for investigating heating due to external perturbations of magnetic field. A current sheet is formed at the resonant surface, which subsequently relaxes after reconnection, forming magnetic islands; a significant amount of initially stored magnetic energy can be released in this way, often more than the energy input by the perturbation itself. However, the nanoflare coronal heating scenario suggests that energy release should occur as a sequence of events. These events may not be independent of each other. Therefore, it is important to investigate the energetics of forced reconnection with a series of driving pulses. Unlike the existing “braiding” numerical experiments,¹⁷ where complex footpoint motions result in quite a complicated magnetic field evolution with many current sheets or filaments appearing, we focus here on magnetic reconnection by considering superposition of elemental reconnective events. This paper is thus a first step, building from individual or elemental reconnection events towards realistic scenarios with many interacting reconnective

tions. The simplicity will prove to be helpful in detailed understanding of the basic physical processes involved. We consider here the situation where a boundary displacement is applied at $t=0$, as in previous work on forced reconnection, but then a subsequent displacement is applied at some later time triggering further reconnection and energy dissipation.

A. Linear theory of multiple pulses

Naive consideration of driving by successive pulses might suggest that the energy release should be expected to be roughly the sum of the energies released by the individual pulses. Consideration of linear theory (valid for small boundary displacements) indicates that this is not the case. For simplicity, assume that we have two driving pulses both of amplitude δ_o and wave number k , as will be investigated in the numerical studies below. According to the linear theory of forced reconnection, the final equilibrium state (the reconnected equilibrium) depends only on the total boundary displacement, so in this case will be given by $\psi_o + \psi_1^{(r)} \times (y, z; k, 2\delta_o)$. That is, the reconnected field is that corresponding to the net boundary displacement which is $2\delta_o$. If the second driving pulse were applied immediately after the first, clearly the initial perturbed state would be given by a perturbed flux function $\psi_1^{(i)}(y, z; k, 2\delta_o)$, that is, the ideal equilibrium for $2\delta_o$, and hence the total energy release would be four times that of a single pulse (not the sum of the individual pulses).

Now, if the second pulse is applied at some later time, whilst the initial current sheet is in the process of relaxing, the magnetic field configuration, and hence the energy input due to the second boundary disturbance, depends on when this occurs. Thus, according to linear theory, the energy release depends on the timing of the pulse, as it is the difference between the energy just after the pulse (which is dependent on the time the pulse occurs) and the energy of the reconnected state (which is independent of the timing of the pulses).

Following Ref. 14, who studied driving by oscillatory boundary motions, we note that the most general equilibrium state of the field is given by a linear combination of the reconnected and ideal equilibria. So long as the boundary displacements are slow compared with an Alfvén time, the field must at any instant be in such an equilibrium state. Thus, just after the second boundary displacement is applied, the perturbed flux function is given by $\psi_1 = \mathcal{A}\psi_1^{(i)} \times (y, z; k, 2\delta_o) + (1 - \mathcal{A})\psi_1^{(r)}(y, z; k, 2\delta_o)$, where the constant \mathcal{A} determines the relative contribution of each equilibrium. Note that we do not expect $\mathcal{A}=1$, as would be the case for the field just after a single pulse, since islands are present just before the second pulse is applied. Immediately following the pulse, there is no time for reconnection to occur and hence the island size (or the value of ψ at the resonant surface) must be unchanged. Thus, \mathcal{A} is determined by the constraint that $\mathcal{A}\psi_1^{(i)}(y, L_z/2; k, 2\delta_o) + (1 - \mathcal{A})\psi_1^{(r)}(y, L_z/2; k, 2\delta_o) = \psi_1(y, L_z/2, t_{pulse})$ where the quantity on the right hand side is the perturbed flux function at the resonant surface at the instant the second pulse is applied. This will be somewhere between 0, if $t_{pulse}=0$, and $\psi_1^{(r)}(y, L_z/2; k, \delta_o)$, if t_{pulse} is large

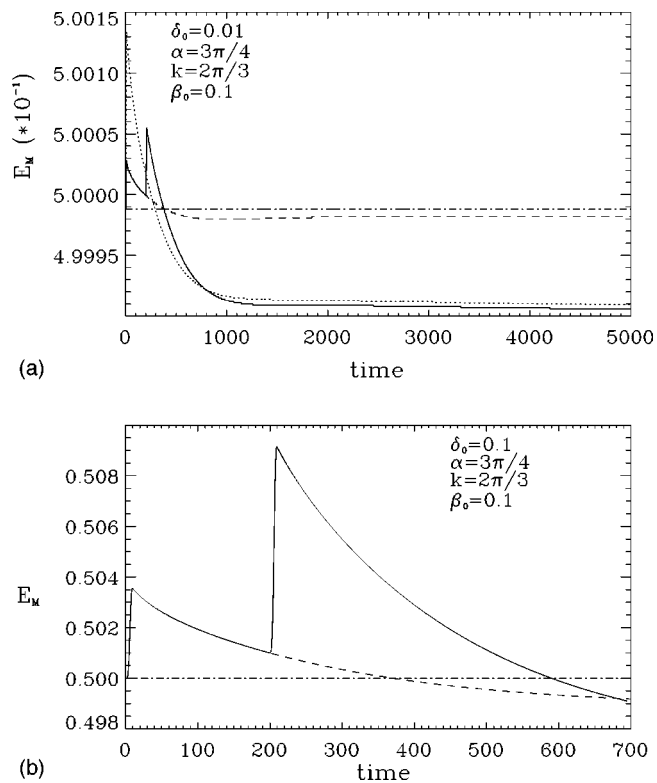


FIG. 6. Averaged magnetic energy E_M as a function of time for “one” pulse (dashed) and “two” pulse (solid) cases (see the text) for (a) $\delta_o=0.01$. The dotted line for the one pulse case for $\delta_o=0.02$ is also shown for comparison (b) same as (a) except $\delta_o=0.1$.

and the field is fully reconnected. It should be noted that the structure of the field, according to linear theory, is just a current sheet at the resonant surface $z=L_z/2$ superimposed on an island chain (whose width depends on the pulse timing). This is shown in Fig. 10 below.

B. Numerical simulations of multiple pulses

As seen in the preceding section, the relaxation time of the field is long compared with the Alfvén time, so it is important to consider the case when a new pulse is applied while the field is still not fully relaxed. Thus, nonlinear effects that originate from the interaction of several pulses will be a significant factor. We apply the first pulse, as before, at $t=0$, but now also apply a second driving pulse at $t=200$. At this time, the field has partially relaxed following the first pulse. The pulses are of the same magnitude δ_o and each comes to rest after ten Alfvén times. In subsequent work, we will consider different δ_o and k .

In Fig. 6, we show averaged magnetic energy E_M versus time for two values of δ_o ; 0.01 and 0.1. In Fig. 6(a), the dashed and dotted curves for $\delta_o=0.01$ and 0.02, respectively, are also shown for comparison for the *one-pulse* case. As seen (solid curves), with the onset of the second pulse (at $t=200$) more magnetic energy is supplied to the system than was supplied by the first pulse. This is entirely consistent with expectations, as described above, since the energies of two pulses add quadratically. For the two-pulse case, even though the system relaxes to similar energy state after the

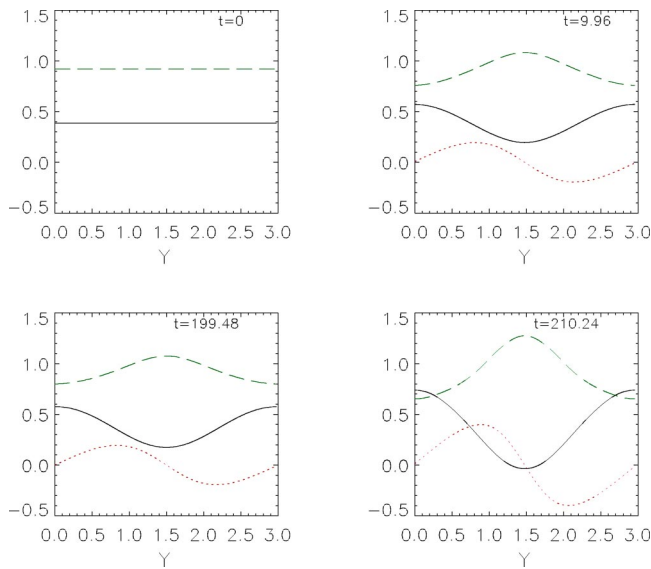


FIG. 7. B_x (solid), B_y (dashed), B_z (dotted) at the boundary $z=0$ for various times t as shown.

reconnection (that is, the reconnected field for a perturbation $2\delta_o$, with small nonlinear modifications), different quantities of energy can be extracted from a perturbation if applied in succession. This also means, as discussed in Sec. III A above, that the energy release depends on the timing of the series of pulses. This is because the magnetic energy release is the difference between the peak of the “spike” (which depends on *when* the pulse is applied) and the reconnected field energy, the eventual steady state (which is almost independent of the pulse timing). In this two-pulse case with $\delta_o=0.01$, the magnetic energy release (difference between the maximum and minimum E_M) just after the first pulse is 2.8×10^{-5} , and 1.5×10^{-4} after the second pulse giving a total energy release of $\sim 1.8 \times 10^{-4}$. In comparison, a single pulse of magnitude $\delta_o=0.02$ releases about 2.2×10^{-4} energy even though the system relaxes to similar energy state after the reconnection. Hence, two separated pulses of same magnitude and wave number release slightly *less* energy than a single combined pulse. Clearly the degree to which the energy is reduced is a function of the timing of the second pulse.

In Fig. 6(b), the magnetic energy release is larger than in Fig. 6(a) because the magnitude of the perturbation applied is large. The dashed line indicates the case when no second pulse is applied and the system relaxes after the first pulse $0 < t \leq 10$. The energy release is also large compared to Fig. 6(a) but the time dependence is not followed long enough for fully reconnected state to be achieved.

It should be noted from Fig. 6 that successive pulses of same magnitude show different energy input because the initial states of the magnetic field (just prior to the pulses) are different. This is illustrated in Fig. 7 where B_x , B_y , and B_z are plotted as a function of y at the boundary ($z=0$) for different times t . When the first pulse is applied at $t=0$, $B_z=0$ and the initial magnetic field determines the start of the Poynting flux. Towards the end (see $t=9.87$) of the first pulse the field components have significantly changed. Now let us consider

the field configuration just before the start of the second pulse, for example, at $t=199.82$. Here, B_z is nonzero and B_x and B_y are quite different from the one when $t=0$. Thus, the initial equilibrium of the system at the start of the second pulse is quite different than at the start of the first pulse, which suggests that the Poynting flux will be different, and hence also the magnetic energy input.

It is interesting to compare the x component of current density J_x and the flux function A_x for *one-* and *two-* pulse cases. Figure 8 shows this comparison where the first and second columns indicate the same time snapshots for $\delta_o=0.1$ when one and two pulses are applied, respectively, at the boundary [see also Fig. 6(b)]. Obviously, the top panel is the same but there are two main differences in the subsequent panels. Strong current densities can be seen along the separatrix for $t=210.7$ just after a second pulse of the same magnitude is applied. Also, the magnetic island widths are large for subsequent times in the case of two pulses. In general, this is not surprising for the following reasons. The latter is entirely consistent with linear theory, see above, which predicts that the reconnected state for two pulses will be the same as that for a single pulse of magnitude $2\delta_o$, and hence the island width will increase by a factor $\sqrt{2}$ if a second pulse is applied. Also, as mentioned in Sec. III A, the general equilibrium configuration for two-pulse case consists of ideal and reconnection equilibrium and hence we expect to see the current sheet and magnetic islands together after the second pulse (right column). In order to see the details and to fully understand any nonlinear effects, we must compare the current densities and flux functions obtained from numerics with the analytical (linear) model. First, we consider the single pulse case. Thus, we compare in Fig. 9 the time snapshots obtained from numerical simulations and the linear theory.¹³ The first column is for one-pulse case obtained from numerics when a perturbation of magnitude $\delta_o=0.1$ was applied for $0 \leq t \leq 10$. The second column shows A_x obtained from the expressions derived in the linear theory¹³ for the same perturbation. Since in linear theory the current density is infinite at the resonant surface and strictly does not show in the gray scale, we have indicated this schematically by a thick, dark line (using a finite width Gaussian profile) on either side of $z=0.5$ in the top panel of the second column. Also, according to the linear theory,¹³ the magnetic island width is $\Delta W \propto \delta_o^{1/2}$, which can be large even for small perturbations. But numerical simulations (here in the bottom panel of column one and in Ref. 15) show that nonlinear saturation of reconnection decreases the island width.

Next, let us compare the two-pulse case of $\delta_o \cos ky$ with the one-pulse case of $2\delta_o \cos ky$. In Fig. 10, first and second column show this, respectively. Clearly, the reconnective equilibrium (bottom panels) are not that different as the final states are very similar. This is in good agreement with linear theory. However, for the top panel it appears that in the two-pulse case, just after the second pulse, the resulting equilibrium with the current density along the separatrix should be close to the superposition of the ideal and reconnected equilibrium as suggested in Sec. III A. To investigate this, we assume that in two-pulse case the boundary has been displaced by $2\delta_o \cos ky$. Next, we need coefficient \mathcal{A} to calcu-

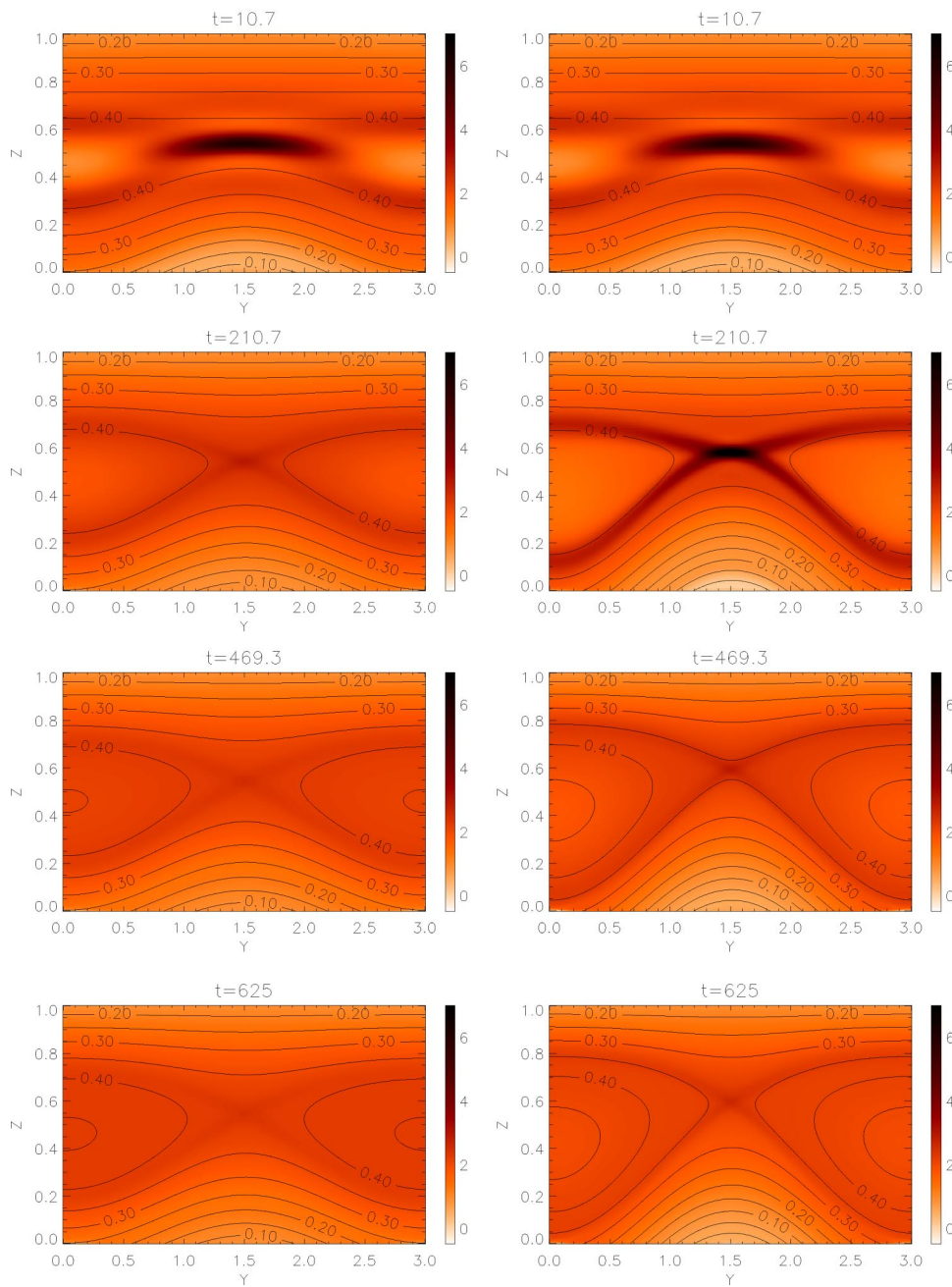


FIG. 8. (Color online). Comparison of current density J_x (color scale) and the flux function A_x (contours) at various times $t=10.7$, 210.7, 469.3, and 625 when one pulse (first column: $0 < t \leq 10$) and two pulses (second column: $0 < t \leq 10$; $200 \leq t \leq 210$) are applied.

late ψ . We calculate the perturbed flux function predicted by linear theory just after the second pulse is applied as explained in Sec. III A. Thus, the perturbed flux function is a linear combination of the “ideal” and “reconnected” equilibria for the net displacement magnitude ($2\delta_o$), with the combination determined by the fact that the degree of reconnected flux is the same as just before the disturbance. This is shown in the third column of Fig. 10, where, as above, the infinite current density sheet is represented graphically as a finite width line. Note that the surprising appearance of the current structure according to linear theory, a current sheet crossing the separatrix, is a simple consequence of the fact that in linear theory perturbations inevitably superpose by simple addition. Thus the formation of the current sheet along the separatrix, a clear feature of the numerical simulations (see first column of Fig. 1), is clearly a nonlinear effect.

On the other hand, the reconnected equilibria for the two pulses (first column) and single pulse of $2\delta_o$ (second column) are very similar, and both are similar to the reconnected equilibrium predicted by linear theory for a $2\delta_o$ displacement (third column). The island widths in the two numerical cases are very slightly reduced by nonlinear effects, consistent with previous results.¹⁵ We then recalculate ψ by using this value of \mathcal{A} and the expressions for $\psi_1^{(i)}$ and $\psi_1^{(r)}$ derived in Refs. 13 and 14. In Fig. 10 (top panel, third column), we plot this ψ which is the linear combination of the ideal and reconnective equilibria for the perturbation of $2\delta_o \cos ky$. The dark line at $z=L_z/2$ is to indicate that the current density is infinitely large according to the linear theory.¹³ The bottom panel in third column is the straightforward reconnective equilibrium calculated using the analytical expression¹³ of

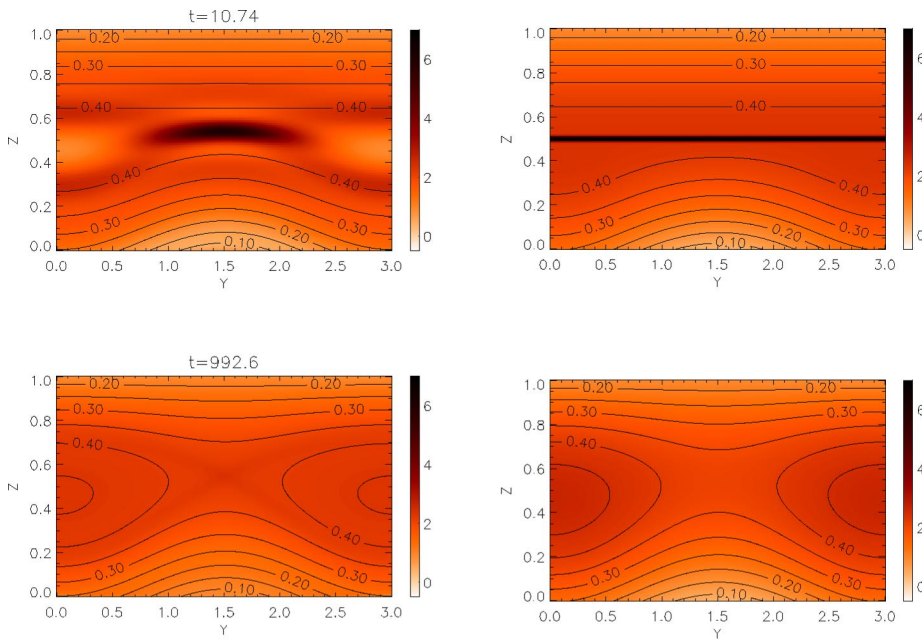


FIG. 9. (Color online). The first column is for $\delta_o=0.1$ for one pulse case where J_x and A_x are obtained from numerics. The second column is $\delta_o=0.1$ and one pulse case where J_x and ψ_x (same as A_x) are calculated from linear theory (Ref. 13).

$\psi_1^{(r)}$ (with pulse magnitude $2\delta_o$). Careful comparison of Figs. 9 and 10 indicate that the presence of a current sheet along the separatrix in the two pulse case is due to the combination of ideal and reconnective equilibrium, as suggested in linear theory,¹⁴ with some modifications due to nonlinear effects.

So far, we have only considered the case of $L_y=3$ (i.e., $k=2\pi/3$). It was predicted in the analytical model¹³ and later confirmed with numerical simulation¹⁵ that the final energy is lower as the region size L_y (wave number k) is longer (smaller). Thus, more energy of the initial field prior to deformation is extracted when a pulse of smaller wave number k is applied. The numerically calculated energy dissipation agrees quite well with the linear theory predictions for inter-

mediate wave numbers k . However, for small k (long wavelengths), the magnetic energy dissipation is found to be reduced compared to the predicted values by the linear theory because close to tearing stability threshold, $(\alpha^2 - k^2)^{1/2} \ll \pi$, perturbations are very large even for small δ_o (see Fig. 4 in Ref. 15). So nonlinear effects are very significant.

In Fig. 11 we show the averaged magnetic E_M as a function of time for various k values when two pulses are applied: $0 < t \leq 10$ and $200 \leq t \leq 210$. As k decreases, the spike of averaged E_M after the second pulse disappears. This is a surprising result, as it conflicts with expectations that the boundary perturbation should produce a Poynting flux into the field and hence give an initial increase in magnetic en-

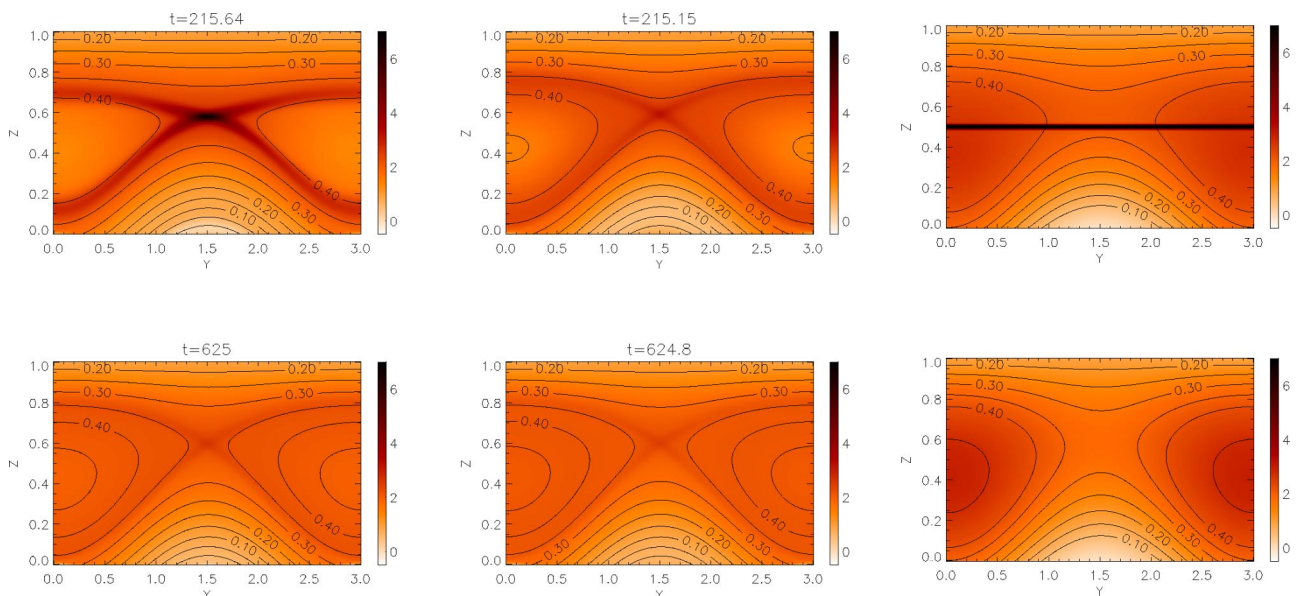


FIG. 10. (Color online). The first column is two-pulse case with $\delta_o=0.1$. The second column is one-pulse case with $\delta_o=0.2$. In both these columns, current density and flux function values are obtained from numerical simulations. The third column is for linear case with $\delta_o=0.2$ (with linear combination of $\psi_1^{(i)}$ and $\psi_1^{(r)}$ in the top panel and reconnective case in the bottom panel (see the text)).

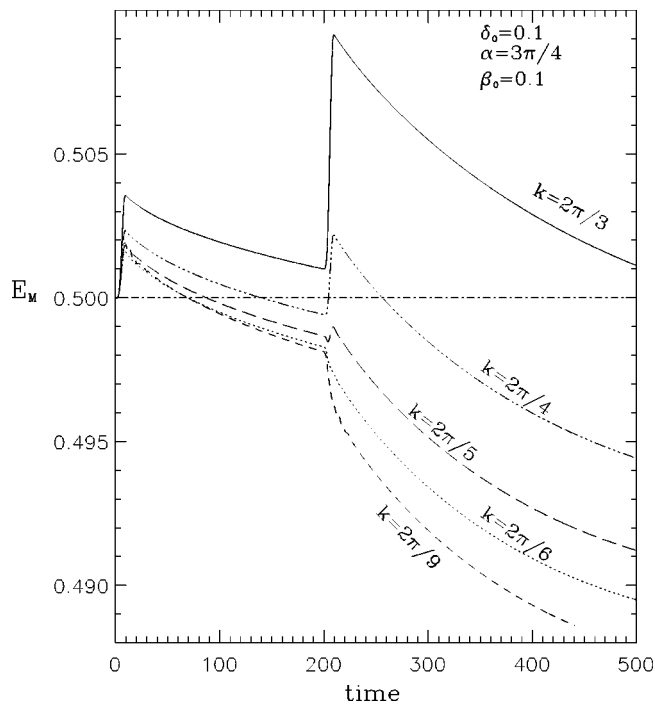


FIG. 11. The average magnetic energy E_M as a function of time for different wave numbers k when the boundary is perturbed by two pulses: $0 \leq t \leq 10$ and $200 \leq t \leq 210$.

ergy (associated with the current sheet formation). In order to see the changes in the current density J_x and flux function A_x just after the second pulse is applied, we plot in Fig. 12 the time snapshots of J_x and A_x for system size $L_y=3$ (top panel), 6 (middle), 9 (bottom panel) for $t \approx 199$ (just before the second pulse was applied) and $t \approx 215$ (some time after the second pulse). Notice that when the second pulse is applied at $t=200$, the field has partially relaxed after reconnection in all three cases (left column), but a short time after the second pulse, the amplitude of the current density increases for larger (smaller) $L_y(k)$ and the current sheet is slightly shifted up from the midplane $z=0.5$. The latter must be a nonlinear effect. The width of the magnetic island is also increased. In short, for smaller k after the second pulse is applied, a much stronger current sheet forms and reconnection occurs rapidly and the averaged E_M curves are dragged down resulting in the disappearance of the spike. This suggests that the nonlinear reconnection rate¹² just after $\sim 50\tau_A$ increases more rapidly after the second pulse. Further investigation of the reasons for this will be a subject of future work.

C. Three pulses

We have analyzed the case of two pulses in detail, but clearly in the solar corona there would be a continual series

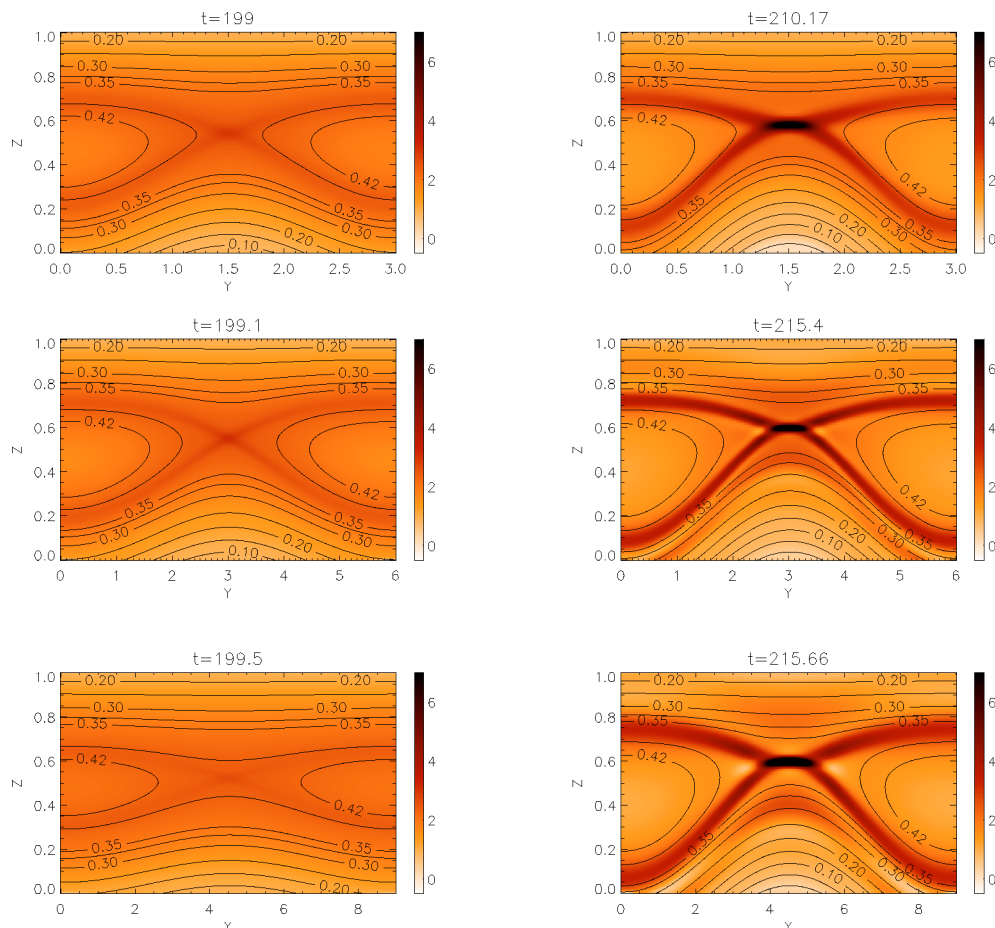


FIG. 12. (Color online). Time development of current density J_x (color scale) and the flux function A_x (contours) for $k=2\pi/3$ (top panels), $2\pi/6$ (middle panels), and $2\pi/9$ (bottom panels) when two pulses are applied (see the text).

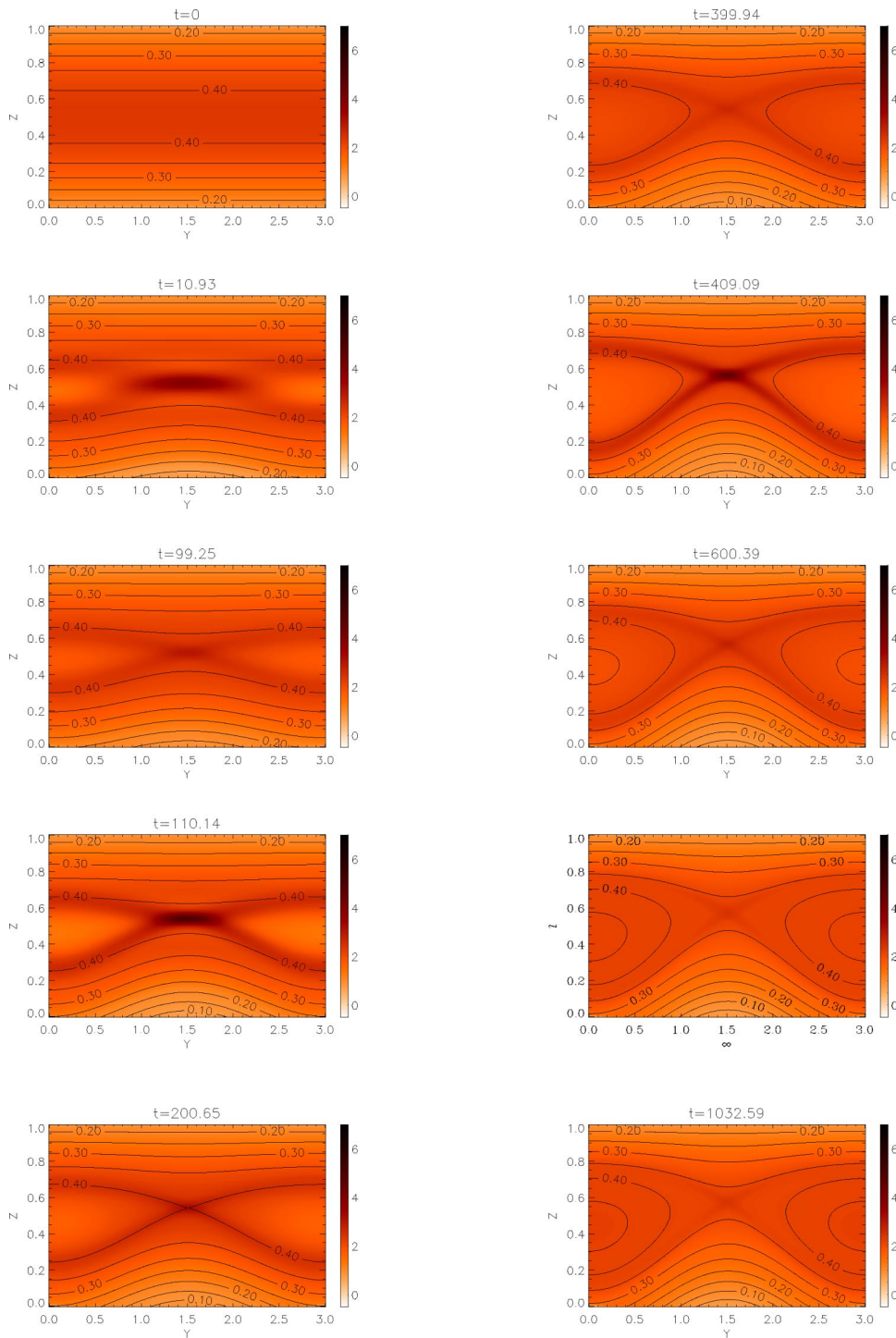


FIG. 13. (Color online). Time development of current density J_x (color scale) and the flux function A_x (contours) when three pulses are applied (see the text).

of heating events which may be randomly distributed in time and magnitude. As a preliminary step towards modeling this, we briefly look at the case of three driving pulses. Multiple pulses will be investigated in more detail in future.

In Fig. 13, we compare the x component of current density J_x and the flux function A_x when three pulses are applied at the boundary: $0 < t \leq 10$, $100 < t < 110$, and $400 < t < 410$. The time development clearly indicates that when the first pulse is applied, the current sheet is formed at the resonant surface and the correspondence between the flux and the current density suggest that the field is in force-free equilibrium. As the second pulse is applied, the current density is more

confined and stronger at the resonant surface. By the time the third pulse is applied, the system has already started to relax with magnetic islands and now the current sheet is quite sharp at the X point.

The averaged (over the simulation domain) magnetic energy versus time for this case is shown in Fig. 14. The solid curves show three peaks of maximum averaged E_M just after each pulse. The dashed and dot-dashed lines are averaged E_M for one-pulse case with $\delta_o = 0.05$ and $\delta_o = 0.15$, respectively. Although pulses of small magnitudes when applied in succession give slightly less magnetic energy compared to a

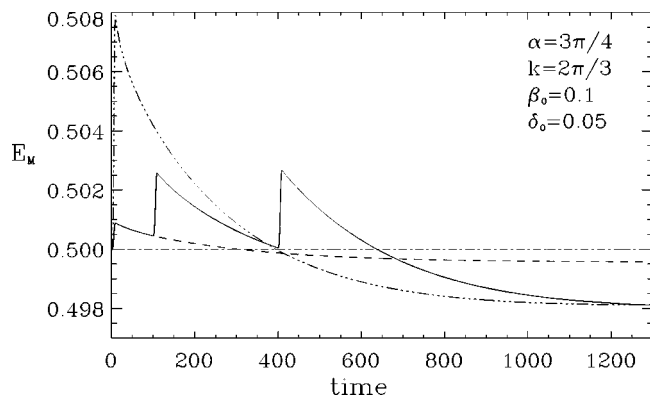


FIG. 14. Averaged magnetic energy E_M as a function of time for one pulse (dashed) and three pulse (solid) case (see the text) for $\delta_o=0.05$. E_M for $\delta_o=0.15$ is also plotted (dot-dashed) for comparison.

single pulse of thrice the magnitude, ongoing current sheet reconnection is a viable dissipation mechanism even for weak but continuous external perturbations.

IV. CONCLUSION

Forced magnetic reconnection is a plausible candidate for solar coronal heating mechanism. Energy release is triggered by boundary disturbances, which initiate current sheet formation and subsequent magnetic reconnection. In the case of the corona, such disturbances will be ubiquitous and may include footpoint displacements or newly emerging flux. A key feature of forced reconnection is that the energy dissipated may be much larger than the energy input from the driving disturbance. Coronal heating is likely to occur as the result of the superposition of many energy release events known as nanoflares. Here, we have made a first step towards modeling this within the forced reconnection scenario by considering heating due to two or more driving pulses, generating a series of energy release events which are not independent of each other. Thus, we have numerically analyzed the magnetic energy release for a two-dimensional, forced magnetic reconnection situation where a highly conducting low β plasma with a sheared force-free field is perturbed by slow pulses at the boundary. This allows nonlinear aspects of the process to be investigated.

For simplicity, we have considered here the case where the pulses have the same wave number. The linear theory of forced reconnection has been extended to deal with this multipulse scenario. This predicts that the final reconnected field state depends on the net boundary displacement, and that just following the second driving pulse, the field is in a linear combination of the ideal and reconnected states, hence having both a current sheet and islands. The magnetic energy release depends on the timing as well as on the magnitude of the successive perturbation. The numerical results agree well with the linear theory concerning the final reconnected state, although nonlinear saturation, due to the finite size of the islands relative to the boundaries, causes a small reduction in island size. However, there is a strong nonlinear effect even for small driving perturbations, in that a current sheet forms

along the already existing separatrix following the second (or subsequent) pulse. The energy release is found to depend on the timing, which has been shown to be due to the dependence of the energy input of the driving perturbation on this factor; in general, the energy release is reduced as the time gap between pulses increases.

The underlying causes of a most intriguing result, that longer wavelengths generate the formation of very strong current sheets and correspondingly faster reconnection, will be the subject of future investigation. A further important topic for future work will be to consider successive pulses of different magnitudes and wavelengths. This could introduce some different effects, as the second driving perturbation will be out of phase with the preexisting island chain, so it is not clear what will be the structure of the second current sheet nor how the energy release of the second pulse will interact with the first.

In the solar corona, the foot-point perturbations due to exploding granules are likely to be continuous and quite possibly randomly distributed. This may be modeled by assuming a random distribution for the magnitudes, width, and the time intervals between the pulses. We will subsequently impose a random distribution of driving pulses to match such granular disturbances and then calculate evolution of the field, including the distribution of the energy-releasing events. This also raises some interesting new issues, since a property of forced reconnection is that each driving pulse releases some stored energy of the initial field (hence acting more as a catalyst than as a primary source of energy). This cannot continue indefinitely, as the energy of the initial field will become depleted. Thus, to maintain a steady heating scenario, there must be some energy supply to replenish the background field.

ACKNOWLEDGMENTS

This work was supported by PPARC, UK. R.J. would like to thank *The Nuffield Foundation* for NUF-NAL 04 award. K.K. also acknowledges the support provided by the JSPS Japan-UK Cooperation Science Program (PI: K Shibata and N. O. Weiss).

- ¹P. K. Browning, *Plasma Phys. Controlled Fusion* **33**, 539 (1991).
- ²U. Narain and P. Ulmschneider, *Space Sci. Rev.* **75**, 453 (1996).
- ³K. J. H. Phillips, *Plasma Phys. Controlled Fusion* **42**, 113 (2000).
- ⁴R. W. Walsh and J. Ireland, *Astron. Astrophys. Rev.* **12**, 1 (2003).
- ⁵E. N. Parker, *Astrophys. J.* **330**, 474 (1988).
- ⁶E. R. Priest and T. Forbes, *Magnetic Reconnection* (Cambridge University Press, Cambridge, 2000).
- ⁷T. S. Hahn and R. M. Kulsrud, *Phys. Fluids* **28**, 2412 (1985).
- ⁸R. Fitzpatrick and T. C. Hender, *Phys. Fluids B* **3**, 644 (1991).
- ⁹X. Wang and A. Bhattacharjee, *Phys. Fluids B* **4**, 644 (1991).
- ¹⁰C. C. Hegna, J. D. Callen, and R. J. La Haye, *Phys. Plasmas* **6**, 130 (1999).
- ¹¹A. Cole and R. Fitzpatrick, *Phys. Plasmas* **11**, 3525 (2004).
- ¹²J. Rem and T. J. Schep, *Plasma Phys. Controlled Fusion* **40**, 139 (1998).
- ¹³G. Vekstein and R. Jain, *Phys. Plasmas* **5**, 1506 (1998).
- ¹⁴G. Vekstein and R. Jain, *Phys. Plasmas* **6**, 2897 (1999).
- ¹⁵P. K. Browning, J. Kawaguchi, K. Kusano, and G. Vekstein, *Phys. Plasmas* **1**, 8 132 (2001).
- ¹⁶K. Kusano (private communication).
- ¹⁷B. V. Gudiksen and A. Nordlund, *Astrophys. J.* **572**, L113 (2002).